Journal of Alloys and Compounds 509 (2011) 2621–2626

Contents lists available at ScienceDirect

Journal of Alloys and Compounds

journal homepage: www.elsevier.com/locate/jallcom

Efficient solid-state route for the preparation of spherical YAG:Ce phosphor particles

C.W. Won [a], H.H. Nersisyan [a,*], H.I. Won [a], J.H. Lee [b], K.H. Lee [c]

[a] RASOM, Chungnam National University, Yuseong, Daejeon 305-764, South Korea
[b] Graduate School of Green Energy Technology, Chungnam National University, 79 Daehak-ro, Yuseong, Daejeon 305-764, South Korea
[c] Department of Nano Materials Engineering, Chungnam National University, Yuseong, Daejeon 305-764, South Korea

ARTICLE INFO

Article history:
Received 28 July 2010
Received in revised form
16 November 2010
Accepted 22 November 2010
Available online 30 November 2010

Keywords:
Oxide materials
Phosphors
Solid state reaction
Luminescence
YAG:Ce

ABSTRACT

The formation of $Y_3Al_5O_{12}:Ce^{3+}$ (YAG:Ce) powders from the corresponding submicrometer-sized oxides and 5 wt% BaF_2 flux is studied at different heating temperatures. The reaction powders are characterized using XRD, SEM, and TEM-EDS. X-ray analysis reveals the sequential formation of the $Y_4Al_2O_9$ (YAM), $YAlO_3$ (YAP), and $Y_3Al_5O_{12}$ (YAG) phases in the temperature range of 1000–1300 °C. It is shown that the nucleation process occurs via the dissolution–precipitation mechanism, whereas the grain growth process is controlled via the liquid-phase diffusion route. YAG:Ce phosphor particles prepared using a proposed technique exhibit a spherical shape, high crystallinity, and an emission intensity that is approximately 10–15% greater than that of commercial phosphor powder.

1. Introduction

Rare-earth-doped yttrium aluminum garnet (YAG) materials are potential phosphor candidates for use in cathode-ray tubes (CRTs), field-emission displays (FEDs), and applications involving scintillation and electroluminescence [1–3]. The development of high-resolution, high-efficiency displays is critically dependent on the properties of the phosphor particles used in their fabrication. Generally, phosphor powders that exhibit a spherical morphology and have uniform diameters of approximately 1–3 μm facilitate the development of high-brightness, high-resolution displays [4].

YAG particles have been produced using several techniques. These include solvothermal synthesis [5–7], hydrothermal synthesis [8–12], metal-organic chemical vapor deposition (MOCVD) [13], co-precipitation [14], spray pyrolysis [15,16], spark-plasma synthesis [17], microwave irritation [18], and sol–gel combustion [19,20]. These chemical processes achieve symmetrical mixing of the precursor materials on the molecular level, lowering the synthesis temperature and promoting the formation of submicron and/or nanosized particles having uniform grain morphology. However, phosphor particles produced using the abovementioned techniques exhibit low emission intensity; this is because the luminescence efficiency of phosphors becomes seriously degraded when the particle size is smaller than 1 μm. Moreover, most of these techniques have inherent disadvantages. These include the requirement of controlling the solution pH, which is difficult; expensive starting materials; and long reaction time. All these factors have contributed to limiting the mass production of phosphors using these techniques.

Powders with pure YAG phase are usually synthesized by a conventional solid-state reaction method with Y_2O_3 and Al_2O_3 as the raw materials [21–23]. This is a cost-effective, efficient method, as compared with other synthesis methods. However, this method has a few inherent disadvantages in that it requires a high calcination temperature and long processing time. These factors contribute to the formation of coarse agglomerated particles, necessitating another process for grinding these agglomerates into particles of sizes on the order of several microns. The resulting extensive ball milling could lead to contamination and degeneration of the luminescent property of the obtained powder. In light of these issues, the present study mainly focuses on developing a solid-state reaction to produce spherical, micrometer-sized YAG:Ce phosphor particles with a low degree of agglomeration. To overcome the drawbacks of the conventional solid-state reaction method and to achieve the desired particle shape and phase purity, we prepare an initial mixture using submicrometer-sized oxide powders (Y_2O_3, Al_2O_3, and CeO_2) combined with BaF_2, which is known as a proper flux in the synthesis of YAG powders [16,24,25]. This paper will also

* Corresponding author at: Practical Application Materials, Chungnam National University, 220 Kung-Dong, Yuseong-gu, Daejeon 305-764, Republic of Korea. Tel.: +82 42 821 6587; fax: +82 42 822 9401.
E-mail address: haykrasom@hotmail.com (H.H. Nersisyan).

0925-8388/$ – see front matter © 2010 Elsevier B.V. All rights reserved.
doi:10.1016/j.jallcom.2010.11.143

Fig. 1. Laboratory box furnace with two alumina crucibles. The smaller crucible contains the reaction mixture, and the larger crucible contains charcoal.

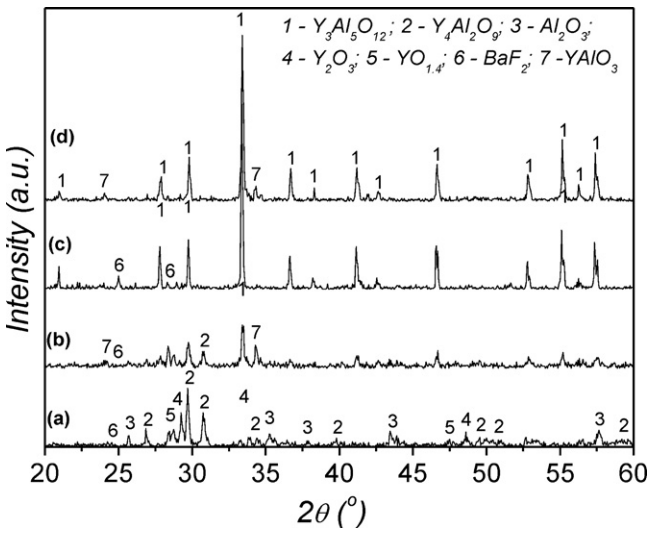

Fig. 2. XRD patterns of YAG:Ce phosphors: (a) 1000 °C, (b) 1150 °C, (c) 1300 °C. For comparison, and (d) XRD patterns of YAG:Ce synthesized at 1300 °C (without BaF_2) are provided.

discuss the basic techniques used in this study to synthesize spherical YAG:Ce phosphor micrometer-sized particles via a modified solid-state reaction, the nucleation process, and the grain growth mechanism.

2. Experimental

The sample used in the present study was prepared such that it had the following overall composition: $Y_{2.95}Ce_{0.05}Al_5O_{12}$. The main starting materials used for preparing the YAG:Ce phosphor were aluminum oxide (Al_2O_3, particle size: 01–0.3 μm, purity: 99.95%); yttrium oxide (Y_2O_3, particle size: <2 μm, purity: 99.99%); cerium oxide (CeO_2, particle size: <1 μm, purity: 99.99%); and barium fluoride (BaF_2, mean particle size: 0.5 μm, purity: 98%). All the starting materials were weighed according to the stoichiometric ratio and mixed in an aqueous medium for several hours using the ball-mill technique. After the powder mixture was dried, it was loosely compacted in an alumina crucible, which was then placed in a larger alumina crucible partially filled with small pieces of charcoal; this created a reducing CO atmosphere to facilitate the $Ce^{4+} \rightarrow Ce^{3+}$ transition. The crucibles were sealed and loaded into a laboratory box furnace. The furnace was heated to the working temperature (1000–1500 °C) at the rate of 300 °C/h. Fig. 1 shows a schematic illustration of the laboratory box furnace with the two alumina crucibles inside it. The reaction mixture in the smaller crucible and charcoal in the larger one are also indicated. The powder mixture sample was maintained at the maximum temperature for 10 min and then allowed to cool naturally. The yellow powder formed after the heat treatment was washed thoroughly with hot water to eliminate BaF_2 and then dried in an oven at 100 °C.

Powder diffraction patterns were recorded using an X-ray diffractometer with Cu Kα radiation (Siemens D5000, Germany). Powder morphology was studied using a transmission electron microscope (TEM, JEM 2010, Japan) and a scanning electron microscope (SEM, JSM 5410, JEOL, Japan). The relative photoluminescent (PL) emission intensities of the samples were measured using a fluorescence spectrophotometer (F-7000, Hitachi, Japan) equipped with a Xe lamp having an excitation wavelength of 450 nm at room temperature.

3. Results and discussion

3.1. Synthesis and characterization

Ce^{+3}-doped YAG samples were prepared via high-temperature calcination of a reaction mixture containing stoichiometric amounts of metal oxides and 5 wt% BaF_2 as a "proper flux". The experiments were conducted at temperatures above and below the melting point of BaF_2 (T_{melt} = 1368 °C). Fig. 2 shows the X-ray diffraction (XRD) patterns of the YAG:Ce phosphors calcinated at different temperatures for 10 min. The XRD patterns of YAG:Ce prepared at 1300 °C without BaF_2 are also provided for comparison. Fig. 2(a) shows that the multiphase product comprising $Y_4Al_2O_9$ (YAM), Al_2O_3, Y_2O_3, $YO_{1.4}$ (yttrium suboxide), and BaF_2 was formed at 1000 °C. No peaks corresponding to the $Y_3Al_5O_{12}$ (YAG) phase were detected at this temperature. For samples calcinated at 1150 °C (Fig. 2(b)), the diffraction peaks indicate the formation of $Y_3Al_5O_{12}$ (YAG), $YAlO_3$ (YAP), and $Y_4Al_2O_9$ (YAM) phases. The concentration of YAG continuously increased with the increase in temperature, leaving behind small amounts of YAM and YAP. When the calcination temperature was increased to 1300 °C, the diffraction peaks of YAM and YAP no longer appeared in the XRD patterns, and phase-pure YAG was obtained (Fig. 2(c)). In the case of the sample calcinated without BaF_2 at 1300 °C, a noticeable amount of YAP remained in the final product (Fig. 2(d)). Normally, YAG is synthesized using coarse precursor powders (via the solid-state route) in the temperature range of around 1500–1600 °C [21–23]. However, in the proposed synthesis route, YAG:Ce is synthesized at a lower temperature because of the small size of the precursor oxides and the addition of BaF_2 as a flux.

TEM analysis of the YAG samples prepared at various temperatures (1250–1500 °C) was carried out to observe the nucleation and growth of particles in the Y_2O_3–Al_2O_3–CeO_2–BaF_2 system. The results of the analysis are shown in Fig. 3. Heat treatment of the reaction mixture at 1250 °C resulted in the formation of a powder having a complex morphology; it consists of a blend of submicrometer-sized spherical particles (dark color) and irregular white fragments, Fig. 3(a). The average diameter of the spherical particles is less than 500 nm, as estimated from a micrograph, Fig. 3(b). The white fragments exhibit a layered texture and are non-uniformly spread over the surface of the spherical particles. To determine the chemical composition of the white fragments and the spherical particles, shown in Fig. 3(a), we carried out transmission electron microscope-energy dispersion spectrum (TEM-EDS) analysis. According to the results of the analysis, the spherical particles consist of Y, Al, and O (Fig. 3(b), point 1), and the white color fragment consists of Ba and F, along with Y, Al, and O (Fig. 3(b), point 2). This observation might possibly indicate the coexistence of two or more phases: the dark phase (spherical particles), consisting of only yttrium–aluminum oxides (most likely $Y_3Al_5O_{12}$), and the white phase, consisting of a mixture of yttrium–aluminum oxides (most likely YAM and/or YAP) and BaF_2. A further increase in the temperature results in the formation micrometer-sized spherical particles with weak aggregation characteristics. Representative TEM images of particles synthesized at 1300 and 1500 °C are shown

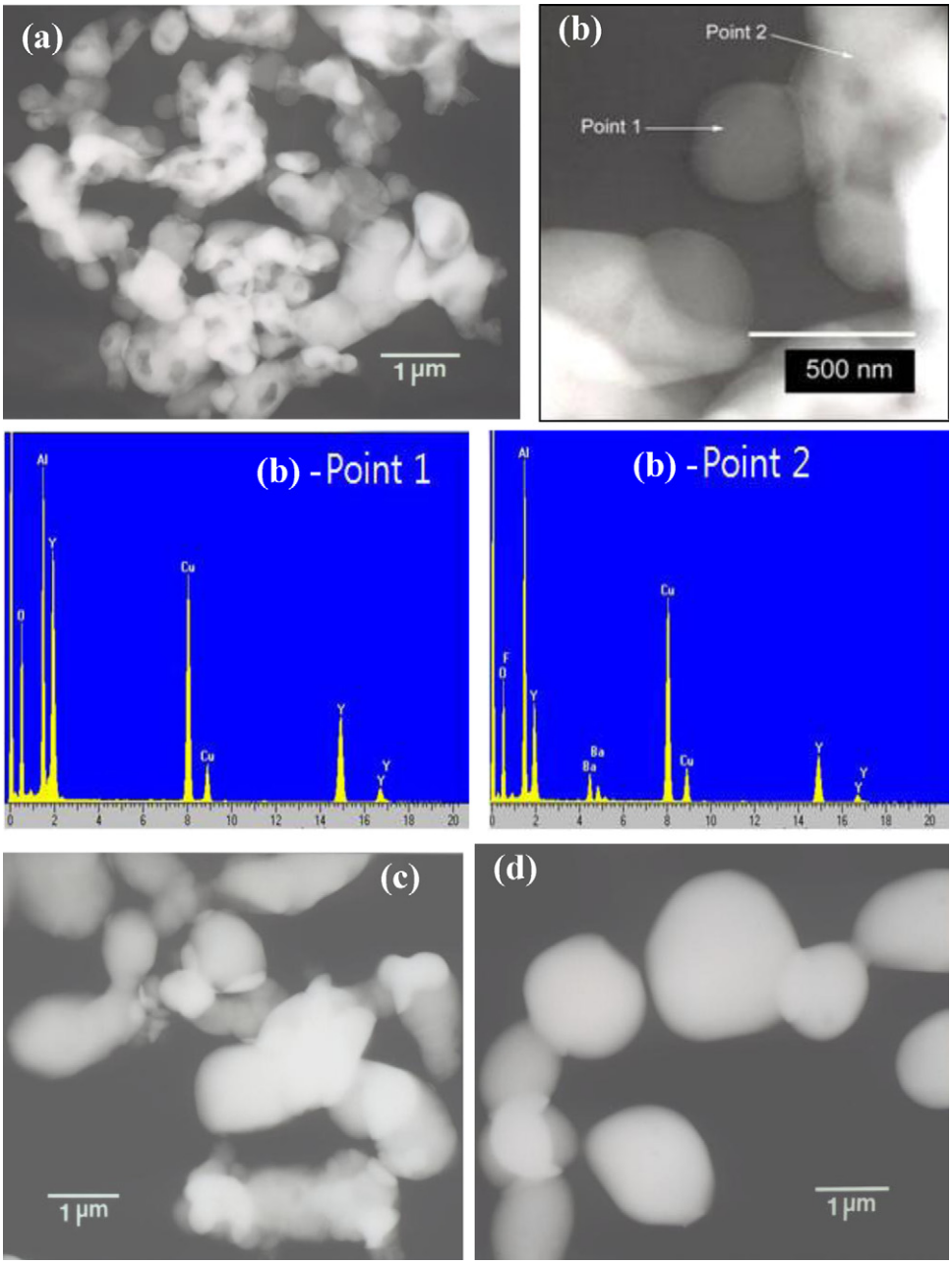

Fig. 3. TEM micrographs of YAG:Ce particles prepared at various temperatures: (a) and (b) 1250 °C; (c) 1300 °C; and (d) 1500 °C. Here, (b) (points 1 and 2) are TEM-EDS element patterns of YAG:Ce particles synthesized at 1250 °C.

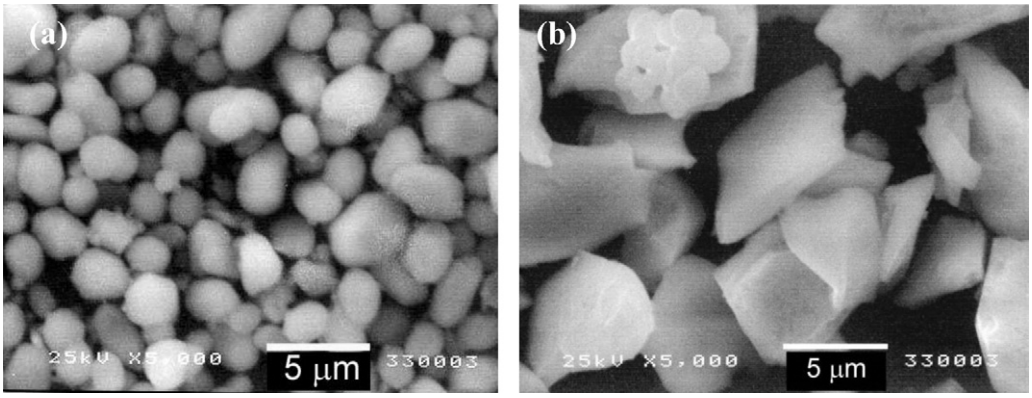

Fig. 4. (a) YAG:Ce powder synthesized at 1500 °C and grinded for a short time, and (b) commercial YAG:Ce sample.

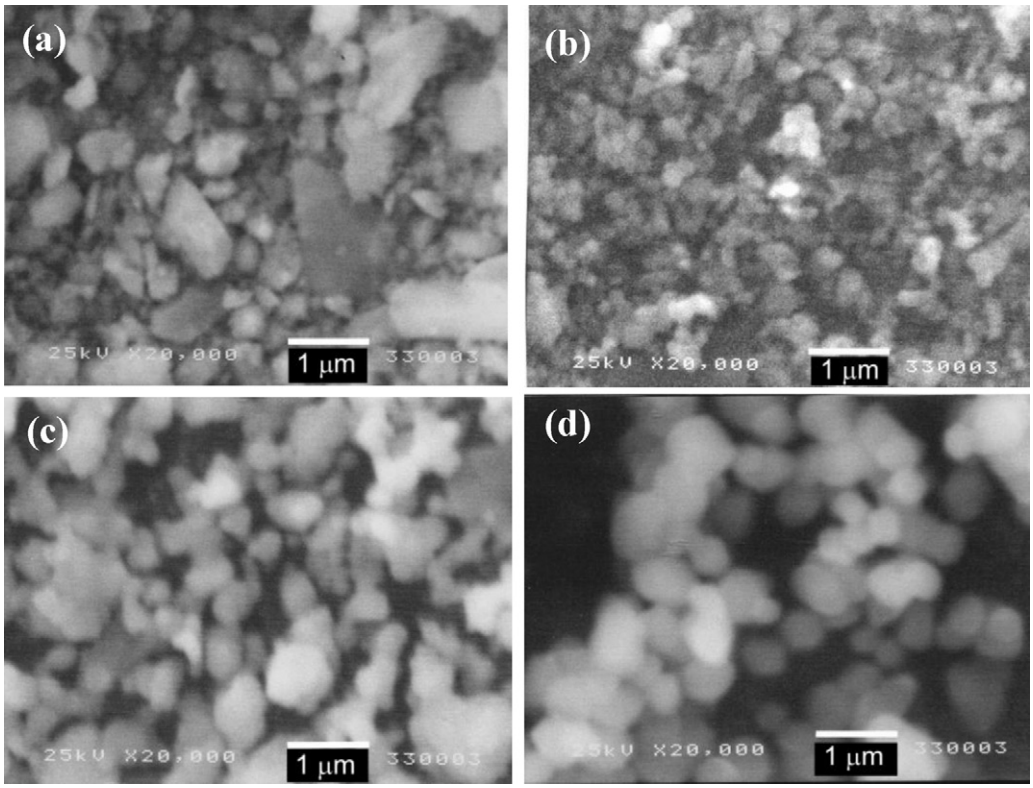

Fig. 5. (a and b) SEM micrographs of Y_2O_3 and Al_2O_3 powders before and (c and d) after calcination at 1250 °C with 5% BaF_2.

in Fig. 3(c) and (d), respectively. The tendency of the particle size to increase can be clearly observed in these micrographs. After the sample was ground for a short duration, having a uniform size distribution was obtained (Fig. 4(a)). The diameter of the particles is in the range of 1–5 μm. For comparison, the SEM image of a commercial YAG sample (Nichia) is shown in Fig. 4(b). As can be seen, a majority of the particles in the commercial sample have an irregular shape because of the high calcination temperature (1600 °C or above) used in their production and the subsequent extreme milling carried out to decrease the subsequent agglomeration. In addition, these particles have a large size (10–25 μm) compared to those obtained using the proposed technique.

3.2. Reaction pathway and mechanism of nucleation and particles growth

From the XRD results, it can be deduced that first, the Al_2O_3-rich $Y_4Al_2O_9$ (YAM) phase is formed by a reaction between fine particles of Y_2O_3 and Al_2O_3. Then, the $YAlO_3$ (YAP) and $Y_3Al_5O_{12}$ (YAG) phases are formed. The formation of $Y_4Al_2O_9$ was detected between 950 and 1000 °C, and this formation can be described as resulting from the combination of Y_2O_3 and Al_2O_3:

$$2Y_2O_3 + Al_2O_3 \rightarrow Y_4Al_2O_9 \quad (1)$$

Increasing the temperature above 1000 °C facilitates the formation of the $YAlO_3$ and $Y_3Al_5O_{12}$ phases. The phase transitions in the 1100–1300 °C temperature range can be expressed by the following reactions:

$$Al_2O_3 + Y_4Al_2O_9 \rightarrow 4YAlO_3 \quad (2)$$

$$3YAlO_3 + Al_2O_3 \rightarrow Y_3Al_5O_{12} \quad (3)$$

It should be noted that the phase transitions in the Y_2O_3–Al_2O_3 system are not confined to only the reactions stated above. The following reactions can be also considered as a part of the given mechanism:

$$Y_2O_3 + Al_2O_3 \rightarrow 2YAlO_3 \quad (4)$$

$$1.5Y_2O_3 + 2.5Al_2O_3 \rightarrow Y_3Al_5O_{12} \quad (5)$$

$$Y_4Al_2O_9 + Y_2O_3 + 4Al_2O_3 \rightarrow 2Y_3Al_5O_{12} \quad (6)$$

The XRD results also indicate that phase transitions occur at 1300 °C, leaving behind pure-phase YAG powder having spherical particles. A further increase in the temperature from 1300 to 1550 °C was found to cause an appreciable increase in the mean particle diameter and enhance the emission intensity of the YAG:Ce phosphor.

There can be two possible reasons for the formation of the YAG phase at a relatively low temperature (1200–1300 °C). One is the accelerated diffusion of Al^{3+} into the Y_2O_3 lattice because of the small size and high reactivity of the initial particles and the other is the liquid phase diffusion and/or dissolution–precipitation processes, which could potentially occur during heat treatment. To clarify this further, we investigated the morphology change in raw oxides after heat treatment at 1250 °C in the presence of 5% BaF_2. The results are shown in Fig. 5. Most of the particles in the initial Y_2O_3 powder are smaller than 1 μm; however, a sufficient number of them are also micrometer-sized (Fig. 5(a)). The initial Al_2O_3 powder consists of uniform particles with a mean diameter of 0.2 μm (Fig. 5(b)). Heat treatment of these powders at 1250 °C causes a significant change in the morphology of the individual oxides: the Y_2O_3 particles appear to coarsen into irregular shapes or agglomerate (Fig. 5(c)), whereas the Al_2O_3 particles are spherical and have diameters of 0.3–0.5 μm (Fig. 5(d)).

This observation indicates that during the heat treatment of the $1.5Y_2O_3 + 2.5Al_2O_3 + 5\%\ BaF_2 + CeO_2$ reaction mixture, Y_2O_3 and Al_2O_3 particles undergo morphological changes as a result of contact with BaF_2. As mentioned above, these particles may form in the liquid phase by the so-called dissolution–precipitation route

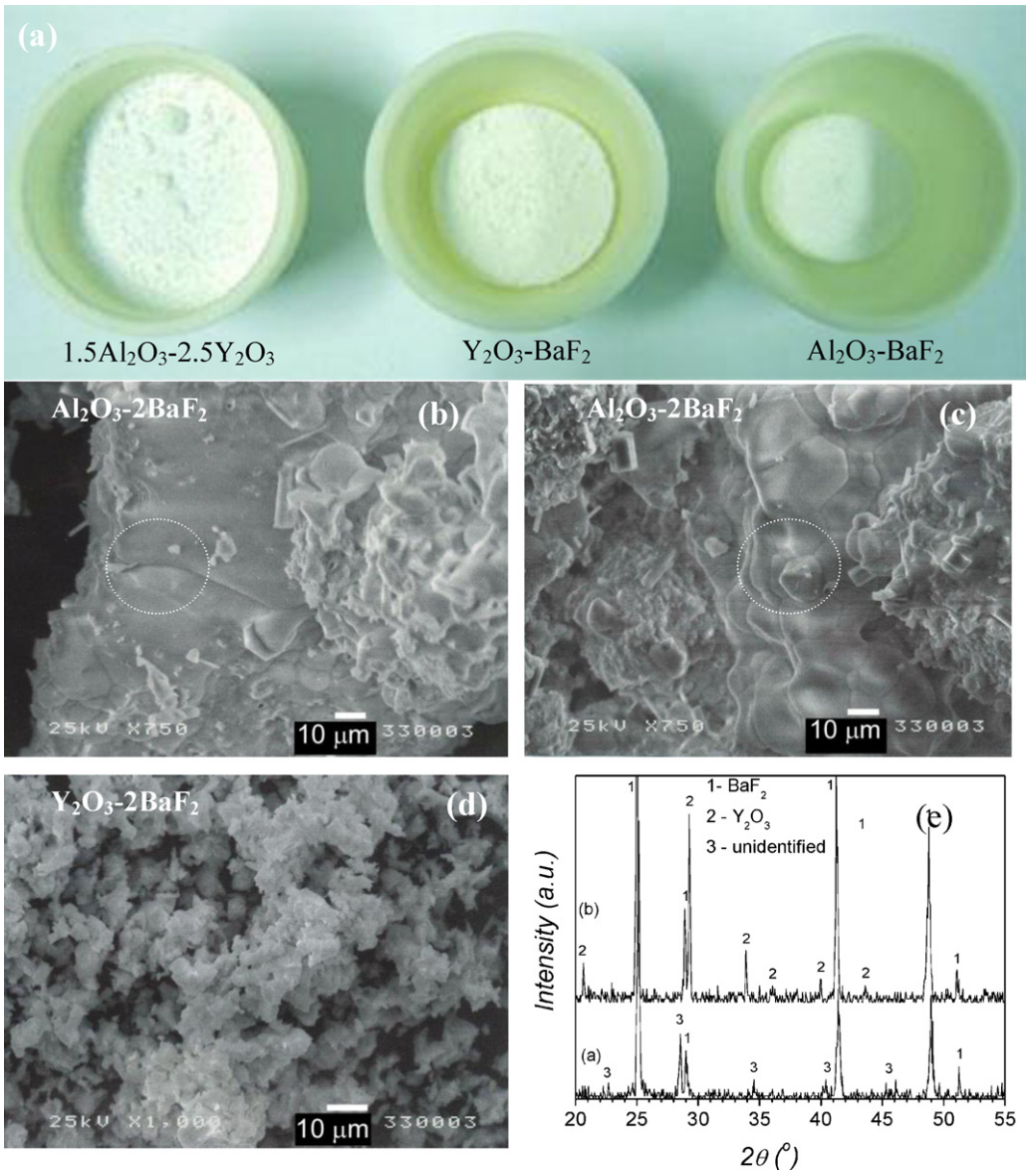

Fig. 6. (a) Alumina crucibles with $1.5Al_2O_3$–$2.5Y_2O_3$, Y_2O_3–BaF_2, and Al_2O_3–BaF_2 mixtures heat-treated at 1250 °C; (b, c, and d) SEM micrographs of Al_2O_3–BaF_2 and Y_2O_3–BaF_2 mixtures heat-treated at 1250 °C; (e) XRD patterns of final products.

and gradually become spherical in shape, as a result of the effect of interfacial tension in the liquid phase. Typically, because the melting points of all the raw materials (Al_2O_3, Y_2O_3, CeO_2, and BaF_2) and the final YAG powder are higher than 1250 °C, none of them will melt at 1250 °C. In fact, the observation and identification of a liquid phase (if any) can be very useful for determining the reaction mechanism. Unfortunately, the concentration of BaF_2 in the reaction mixture is only 5%, and thus, the portion of BaF_2 that is expected to be in the liquid phase will be small and difficult to detect by SEM analysis. Therefore, we prepared two binary mixtures with an Y_2O_3–BaF_2 (1:1) and Al_2O_3–BaF_2 (1:1) composition and heat-treated them at 1250 °C. In Fig. 6, the photographs of the powders after the heat treatment are shown along with the corresponding XRD and SEM analyses data. No shrinkage can be observed for the Y_2O_3–Al_2O_3 powder after heat treatment (Fig. 6(a), left-side crucible). The Y_2O_3–BaF_2 mixture shows significant shrinkage (middle crucible), but the shrinkage is almost twice as small as that in the case of the Al_2O_3–BaF_2 mixture. The SEM micrograph in Fig. 6(b) shows a large molten fragment for the Al_2O_3–BaF_2 mixture (selected area). Further, a crystallization process resulting from the observed liquid phase is clearly seen in Fig. 6(c). After the heat treatment, the Y_2O_3–BaF_2 mixture consists of aggregated crystalline particles and no liquid-phase fragments, as can be seen in Fig. 6(d). According to the XRD analysis data, the product produced from Y_2O_3–BaF_2 mixture consists of Y_2O_3 and BaF_2 phases (Fig. 6(e), line b). Meanwhile, the product obtained from the Al_2O_3–BaF_2 mixture contains only BaF_2 and an unidentified phase; no Al_2O_3 peaks are detected in the XRD patterns. It is likely that the Al_2O_3 and BaF_2 reacted together, to yield a product having a low melting point; the unidentified peaks in the XRD patterns could be due to this product. This product could possibly be a fluoride- and oxygen-containing solid solution, fluoride glass, or a double metal fluoride. However, further studies must be conducted to satisfactorily clarify this issue.

The above observations imply that a liquid phase forms at an early stage of the calcination, and the formation of spherical YAG particles occurs by the dissolution–precipitation route. After the dissolution–precipitation process is complete, the grains start interacting with one another; the interactions increase with temperature, as shown in Fig. 3.

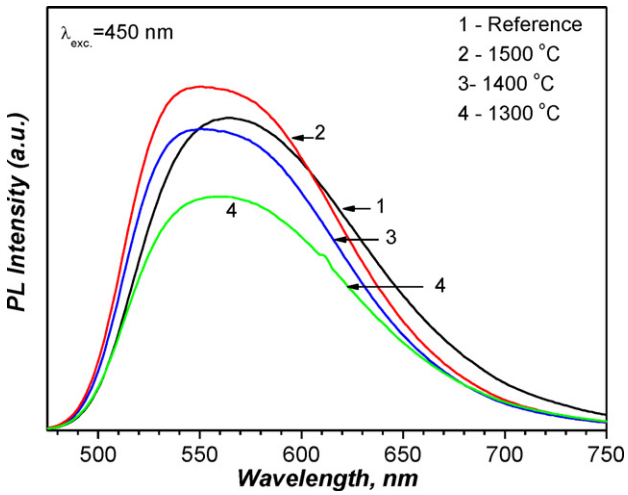

Fig. 7. PL intensity of YAG:Ce powders prepared at different temperatures.

3.3. Luminescence studies

The luminescent spectra of spherical YAG:Ce samples synthesized at different temperatures are shown in Fig. 7. The PL spectra of a commercial YAG:Ce^{3+} sample is provided for comparison. All the emission spectra were detected at an excitation wavelength of 450 nm. The curves denote emissions in the range of 450–800 nm, with a luminescent maximum at 556 nm, attributed to the Ce^{3+} inter-shell transition ($5d \rightarrow 4f$) in the YAG lattice. Higher-intensity emissions were detected in the case of powders treated at 1500 °C. When the firing temperature is below 1500 °C (e.g., 1400 °C and 1300 °C), the obtained phosphor samples exhibit relatively low-intensity emission because of the low crystallinity of the particles and inadequate doping with Ce^{+3}. Remarkably, when the firing temperature is 1500 °C, YAG:Ce is completely synthesized, and the sample emission intensity is 10–15% higher than that of the commercial (reference) sample. Thus, it appears that the proposed method can be adopted to synthesize highly crystalline YAG having small-sized particles with uniformly distributed Ce^{+3} ions in the crystal lattice, and hence, good PL characteristics.

4. Conclusions

Spherical, micrometer-sized polycrystalline $Y_3Al_5O_{12}:Ce^{3+}$ (YAG:Ce) particles having good luminescence properties were synthesized via a solid-state processing route from the corresponding submicrometer-sized oxides and 5 wt% BaF_2 flux. The reaction mixture was heat-treated in the temperature range of 1000–1500 °C to enhance the crystallinity of the yttrium–aluminum garnet phase. SEM and TEM examinations and subsequent morphological analysis using TEM-EDS were carried out to study the nucleation and the grain growth process of the YAG particles in the presence of flux. It was shown that the nucleation of spherical YAG particles occurs via the dissolution–precipitation mechanism, whereas the grain growth process is controlled via the liquid-phase diffusion route. The YAG:Ce phosphor powder prepared at 1500 °C had an emission intensity approximately 10–15% higher than that of commercial phosphor powder.

Acknowledgments

This research was supported by the Basic Science Research Program through the National Research Foundation of Korea (NRF) funded by the Ministry of Education, Science and Technology (2010-0794).

References

[1] K. Zhang, H.Z. Liu, Y.T. Wu, W.B. Hu, J. Alloys Compd. 453 (2008) 265.
[2] V. Lupei, J. Alloys Compd. 451 (2008) 52.
[3] M. Nakielska, J. Sarnecki, M. Malinowski, R. Piramidowicz, J. Alloys Compd. 451 (2008) 190.
[4] A. Ikesue, T. Kinoshita, J.H. Lee, T. Mori, Y. Yajima, J. Mater. Res. 15 (2000) 1864.
[5] Y. Sanga, H. Liua, Y. Lva, J. Wanga, T. Chena, D. Liu, X. Zhang, H. Qin, X. Wang, R.I. Boughton, J. Alloys Compd. 490 (2010) 459.
[6] X.D. Zhang, H. Liu, W. He, J.Y. Wang, X. Li, R.I. Boughton, J. Cryst. Growth 275 (2005) 1913.
[7] Z. Wu, X. Zhang, W. He, Y. Du, N. Jia, P. Liu, F. Bu, J. Alloys Compd. 472 (2009) 576.
[8] Y. Hakuta, T. Haganuma, K. Sue, T. Adschiri, K. Arai, Mater. Res. Bull. 38 (2003) 1257.
[9] H. Yang, L. Yuan, G. Zhu, A. Yu, H. Xu, Mater. Lett. 63 (2009) 2271.
[10] J.H. In, H.C. Lee, M.J. Yoon, K.K. Lee, J.W. Lee, C.H. Lee, J. Supercrit. Fluids 40 (2007) 389.
[11] M.J. Yoon, J.H. In, H.C. Lee, C.H. Lee, Korean J. Chem. Eng. 23 (2006) 842.
[12] Q.X. Zheng, B. Li, H.D. Zhang, J.J. Zheng, M.H. Jiang, X.T. Tao, J. Supercrit. Fluids 50 (2009) 77.
[13] Y. Li, J. Zhang, Q. Xiao, R. Zeng, Mater. Lett. 62 (2008) 3787.
[14] X. Li, W. Wang, Powder Technol. 196 (2009) 26.
[15] L. Mancic, K. Marinkovic, B.A. Marinkovic, M. Dramicanin, O. Milosevic, J. Eur. Ceram. Soc. 30 (2010) 577.
[16] S.H. Lee, D.S. Jung, J.M. Han, H.Y. Koo, Y.C. Kang, J. Alloys Compd. 477 (2009) 776.
[17] M. Suareza, A. Fernandez, J.L. Menendez, R. Torrecillas, J. Alloys Compd. 493 (2010) 391.
[18] M.L. Saladino, G. Nasillo, D.C. Martino, E. Caponetti, J. Alloys Compd. 491 (2010) 737.
[19] L. Yang, T. Lu, H. Xu, N. Wei, J. Alloys Compd. 484 (2009) 449.
[20] H. Jiao, Q. Ma, L. He, Z. Liu, Q. Wu, Powder Technol. 198 (2010) 229.
[21] Q. Zhang, F. Saito, Powder Technol. 129 (2003) 86.
[22] Y.X. Pan, M.M. Wu, Q. Su, Mater. Sci. Eng. B 106 (2004) 251.
[23] Y.C. Kang, H.S. Roh, S.B. Park, Adv. Mater. 12 (2000) 451.
[24] S.H. Lee, H.Y. Koo, D.S. Jung, J.M. Han, Y.C. Kang, Opt. Mater. 31 (2009) 870.
[25] S. Xu, L. Sun, Y. Zhang, H. Ju, S. Zhao, D. Deng, H. Wang, B. Wang, J. Rare Earth 27 (2009) 327.